Turbulence Modeling Around Extremely Large Cylindrical Bluff Bodies

Andrew Li Jian Pang[1], Martin Skote[1], Siow Yong Lim[2]

[1]School of Mechanical and Aerospace Engineering,
Nanyang Technological University
Singapore

[2]School of Civil and Environmental Engineering,
Nanyang Technological University
Singapore

ABSTRACT

Various turbulence models are analyzed in order to determine the optimal approach to numerically modeling the flow around an extremely large cylindrical bluff body, such as that of an offshore wind turbine foundation. In particular, we focus our study on the Reynolds-Average one- and two-equation turbulence models. These models are less computationally expensive and can be run on workstations that are widely available to engineers. Based on our analysis, we propose best practices on modeling the flow around large cylindrical bluff bodies using the Reynolds-Averaging approaches.

KEY WORDS: Cylinder, Bluff Bodies, CFD, Turbulence, RANS, URANS

INTRODUCTION

In many offshore industries, understanding the fluid flow around a marine structure is an area of high importance. Such an understanding will provide accurate predictions of the loading and responses of the structure due to the fluid flow, as well as insights into various hydraulic processes such as scouring. The sizes of these marine structures can range from relatively narrow risers to extremely wide monopile foundations. While the flow around a narrow cylindrical body is relatively well studied, less can be said about extremely large cylindrical bodies which have a corresponding high Reynolds number flow (Re = 10^6 – 10^7). This results in uncertainties when predicting such flows in practical engineering, especially for the offshore wind turbine industry where a monopile foundation diameter ranges from 4m to 5m wide. Furthermore, with this industry looking at scaling up the wind turbines to 10 MW, there is a likelihood that the diameter of future wind turbine foundation will similarly increase.

One of the main reasons for this gap in our understanding of high Reynolds number flow is due to the size limitation of laboratory experimental setups and the fluid compressibility effects. Currently, experimental data of one of the highest Reynolds number flow (Re = 1.87×10^7) was obtained by Jones *et al.* (1969) using Langley transonic dynamics tunnel. However, there are very few works that have been done within this Re = 10^7 range due to the significant challenges involved. The bulk of available experimental data for such high Reynolds number flow falls within the 10^4 – 10^6 range (Achenbach, 1968; Gunter, 1983; James et al, 1980; Schmidt, 1966).

With the advancement of computational speed and capabilities, numerically modeling the flow around a cylindrical body at high Reynolds number has become increasingly possible, especially in the industry. While ideally, a full Direct Numerical Simulation (DNS) should be used to simulate such a flow, the fine mesh required makes such a simulation not feasible even with current computational capabilities. The next closest alternative will be to perform a Large Eddy Simulation (LES) or a Detached-Eddy Simulation (DES). Squires *et al.* (2008) performed simulations using a DES and DDES (Delayed Detached-Eddy Simulation) turbulence model for the flow around a cylindrical bluff body. The study showed that the DES and DDES models agreed reasonably well with experiments and both models gave approximately identical results. A similar study was done by Catalano *et al.* (2003) using a LES approach and it was shown that the results from the LES simulation correlated well with experiment data for Re = 1×10^6. However, extending the Reynolds number to Re= 2×10^6, Catalano *et al.* (2003) noted that the discrepancy between the simulation results and experimental data increased due to the lack of grid resolution at the wall surface. Hence, even with current computational capabilities, the grid requirement is still the limiting factor when modeling a high Reynolds number flow around a cylinder.

A popular approach to model a turbulent flow on a relatively coarser grid is the Reynolds-Averaged Navier-Stokes (RANS) approach. While there have been some earlier works done on using the RANS approach to model the flow around the cylinder, most of these works focused on lower Reynolds numbers. For very high Reynolds number flow within the range of Re = 10^6, two recent works which were conducted are Catalano *et al*. (2003) and Ong *et al*. (2009), both using the standard k-ε model. For Ong *et al*. (2009), they concluded that the k-ε model is a reliable model for engineering purposes. However, they did highlight that the strong anisotropy of the turbulence in such a flow resulted in some inaccuracy of the simulation results. While the standard k-ε model is a very popular closure model for the RANS approach, there are other one- and two-equation closure models, such as the Spalart-Allmaras and the k-ω models, which can also be applied to such flows. Unal and Goren (2006) conducted a comparative study of the different RANS models in the sub-critical flow range (Re = 10^4). However, currently there seems to be no similar studies done for the trans-critical flows regime which have a very high Reynolds number within the Re = 10^6 range.

Hence, the objective of this work was to perform a comparative study of one- and two-equation RANS turbulence models to determine the best approach when modeling the flow around an extremely large cylindrical bluff body where Reynolds number is very high. Being aware that there is a host of one- and two-equation turbulence models available in literature, this work will focus on the turbulence models which are available in the commercial software FLUENT 14 due to its popularity among many engineers. In addition, this study will be directed toward the offshore wind turbine industry where the understanding of such a flow is critical for their large monopile foundations. Hence, the simulation setup in this work was modeled after the Scroby Sand Wind Farm (DECC, 2008) in the UK. At this wind farm, the turbine monopile foundation is 4.2 m wide and the average prevailing current in the area is approximately 1.25 m/s.

TURBULENCE MODELING

RANS Approach

The RANS approach uses the Reynolds decomposition to define the instantaneous flow property. This instantaneous flow property can be characterized as the superposition of its steady mean component (Φ) and its time varying fluctuating component (ϕ') as shown in Equation 1.

$$\phi = \Phi + \phi' \tag{1}$$

Substituting this Reynolds decomposition equation into the Navier Stokes equation and taking the time average, the resultant continuity and momentum equation are:

$$\frac{\partial u_i}{\partial x_i} = 0 \tag{2}$$

$$\rho\left(\frac{\partial u_i}{\partial t} + \frac{\partial u_i u_j}{\partial x_j}\right) = -\frac{\partial p}{\partial x_i} + \frac{\partial}{\partial x_i}\left(\mu\left(\frac{\partial \mu_i}{\partial x_j} + \frac{\partial u_j}{\partial x_i} - \frac{2}{3}\delta_{ij}\frac{\partial u_l}{\partial x_l}\right)\right) + \frac{\partial\left(-\rho\overline{u_i' u_j'}\right)}{\partial x_j} \tag{3}$$

This equation has a similar form to the original Navier Stokes equation, where u_i and u_j are the mean velocities. However, an additional unknown stress term, called the Reynolds Stresses ($-\rho\overline{u_i' u_j'}$), will appear which results in an open set of equations.

There are two main approaches to model this Reynolds stresses, which is the Boussinesq approach and the Reynolds Stress Transport Model (RSM). In this work, the RSM approach will not be discussed and the Boussinesq approach will be used to model the Reynolds stresses:

$$-\rho\overline{u_i' u_j'} = \mu_t\left(\frac{\partial u_i}{\partial x_j} + \frac{\partial u_j}{\partial x_i}\right) - \frac{2}{3}\left(\rho k + \mu_t \frac{\partial u_k}{\partial x_k}\right)\delta_{ij} \tag{4}$$

Using this Boussinesq approach, additional transport equations must be solved to obtain the turbulent viscosity (μ_t), in Equation 4. The number of additional transport equations that are needed depends on the turbulence model chosen. In this work, we'll focus only on the one-equation (Spalart-Allmaras model) and two-equation (k-ε model and k-ω models) turbulence models. In addition, an Unsteady-RANS (URANS) model, which retains the transient terms of the RANS equation, will be used for all the simulations performed.

One-equation models

The Spalart-Allmaras model (Spalart and Allmaras, 1992) is a one-equation closure model that was originally developed for aerospace applications which experiences adverse wall-bounded flows. In this model, the transport equation shown in Equation 5 is used to solve the kinematic eddy viscosity ($\tilde{\nu}$).

$$\frac{\partial}{\partial t}(\rho\tilde{\nu}) + \frac{\partial}{\partial x_i}(\rho\tilde{\nu}u_i) = G_\nu + \frac{1}{\sigma_{\tilde{\nu}}}\left[\frac{\partial}{\partial x_j}\left\{(\mu + \rho\tilde{\nu})\frac{\partial \tilde{\nu}}{\partial x_j}\right\} + C_{b2}\rho\left(\frac{\partial \tilde{\nu}}{\partial x_j}\right)^2\right] - Y_\nu + S_{\tilde{\nu}} \tag{5}$$

where G_v and Y_v represent the production and destruction of turbulent viscosity, $\sigma_{\tilde{\nu}}$ and C_{2b} are constant and $S_{\tilde{\nu}}$ is a user-define source term. Using the kinematic eddy viscosity ($\tilde{\nu}$), the turbulence viscosity (μ_t) can be determined using Equation 6 which will subsequently be used in the Boussinesq hypothesis.

$$\mu_t = \rho\tilde{\nu}f_{v1} \tag{6}$$

where f_{v1} is the viscous damping function.

In the original Spalart-Allmaras model, it was assumed that turbulence production was based only on the magnitude of the vorticity. Hence in this work, we shall call this model the Spalart-Allmaras (Vorticity) model. However, since then, the importance of taking into account the effects on mean strain in the turbulences production has been acknowledged and modifications to the Spalart-Allmaras model were proposed by Dacles-Mariani *et al.* (1995). We shall call this modified model as the Spalart-Allmaras (Strain/Vorticity) in this work.

At the wall boundary, the Spalart-Allmaras model uses a laminar stress-strain relationship which requires the viscosity-dominated area to be well defined. However, for unresolved viscous sub-layers, FLUENT employs the law-of-the-wall, hence allowing a coarse grid to be used for such a model.

Two-equation models

The k-ε and k-ω models are popular two-equation models which solve the turbulent viscosity (μ_t) by modeling the transport equations of either the turbulence kinetic energy (k) and turbulence dissipation rate (ε) or the turbulence kinetic energy (k) and specific dissipation rate (ω).

For the standard k-ε model (Launder and Spalding, 1972), it is a semi-empirical formula whereby the turbulence kinetic energy (k) was derived from an exact equation and the turbulence dissipation rate (ε) was determined using physical reasoning. The k and ε transport equations are:

$$\frac{\partial}{\partial t}(\rho k) + \frac{\partial}{\partial x_i}(\rho k u_i) = \frac{\partial}{\partial x_j}\left[\left(\mu + \frac{\mu_t}{\sigma_k}\right)\frac{\partial k}{\partial x_j}\right] + G_k + G_b - \rho\varepsilon - Y_M + S_k \tag{7}$$

$$\frac{\partial}{\partial t}(\rho\varepsilon) + \frac{\partial}{\partial x_i}(\rho\varepsilon u_i) = \frac{\partial}{\partial x_j}\left[\left(\mu + \frac{\mu_t}{\sigma_\varepsilon}\right)\frac{\partial \varepsilon}{\partial x_j}\right] + C_{1\varepsilon}\frac{\varepsilon}{k}(G_k + C_{3\varepsilon}G_b) - C_{2\varepsilon}\rho\frac{\varepsilon^2}{k} + S_\varepsilon \tag{8}$$

where G_k and G_b represent the generation of turbulence kinetic energy, Y_M represents the contribution of the fluctuating dilatation in compressible turbulence to the overall dissipation rate, σ_k and σ_ε are the turbulence Prandtl numbers, $C_{1\varepsilon}$, $C_{2\varepsilon}$ and $C_{3\varepsilon}$ are constants and S_k and S_ε are user-defined source terms. Using k and ε, the turbulent viscosity (μ_t) is subsequently solved using Equation 9.

$$\mu_t = \rho C_\mu \frac{k^2}{\varepsilon} \tag{9}$$

where C_μ is a constant.

From the experience gained, numerous works have been done to improve the standard k-ε model further. Two of such improved models are the RNG k-ε model and the realizable k-ε model. The RNG k-ε model (Yakhot and Orszag, 1986) was derived using the statistical renormalization group theory. The resultant model improved the ε transport equation for rapidly strain flow and is also able to account for the effects of swirling flow. In addition, an analytical formula was obtained for the turbulent Prandtl number as compared to a user-defined constant in the standard k-ε model.

The realizable k-ε model (Shih *et al.*, 1995) is another of such improvements to the original standard k-ε model. This model modified the turbulent viscosity formulation and also derived a new ε transport equation from an exact equation. The resultant model satisfies mathematical constraints on the Reynolds stresses which are consistent with the physics of the turbulent flow, hence making the model "realizable". The realizable k-ε model improved the accuracy of predicting the spreading rate of planar and round jets as well as flows with adverse pressure gradients and separation.

As the k-ε model was developed for turbulent core flows, a wall function is needed to model the near wall regions. There are numerous wall functions currently available, but in this work a standard wall function (Launder and Spalding, 1974) was used for all k-ε model simulations performed. In the standard wall function, for a fine grid (y^* < 11.225 at the wall-adjacent cell), a laminar stress-strain relationship is applied at the near wall region. However, when a coarse grid is applied (y^* > 11.225 at the wall-adjacent cell), the law-of-the-wall will be employed instead. In FLUENT, it must be noted that a y^* rather than a y^+ wall unit is used where by y^* is given by Equation 10.

$$y^* \equiv \frac{\rho C_\mu^{1/4} k_P^{1/2} y_p}{\mu} \tag{10}$$

where C_μ is a constant, k_p is the turbulence kinetic energy at that point location, y_p is the distance from the point location to the wall and μ is the dynamics viscosity of the fluid.

Similar to the k-ε model, the k-ω model uses the k and ω transport equations to determine the turbulent viscosity (μ_t) which will subsequently be substituted into the Boussinesq hypothesis. The standard or Wilcox k-ω model (Wilcox, 1988) is an empirical based model with the k and ω transport equations:

$$\frac{\partial}{\partial t}(\rho k) + \frac{\partial}{\partial x_i}(\rho k u_i) = \frac{\partial}{\partial x_j}\left[\Gamma_k \frac{\partial k}{\partial x_j}\right] + G_k - Y_k + S_k \tag{11}$$

$$\frac{\partial}{\partial t}(\rho \omega) + \frac{\partial}{\partial x_i}(\rho \omega u_i) = \frac{\partial}{\partial x_j}\left[\Gamma_\omega \frac{\partial \omega}{\partial x_j}\right] + G_\omega - Y_\omega + S_\omega \tag{12}$$

where G_k and G_ω represent the generation terms of k and ω, Y_k and Y_ω represent the dissipation terms of k and ω, Γ_k and Γ_ω represents the effective diffusivity of k and ω, and finally S_k and S_ε are the user-defined source terms. The turbulent viscosity (μ_t) is subsequently determined using:

$$\mu_t = \alpha^* \frac{\rho k}{\omega} \tag{13}$$

where α^* is the damping coefficient of the turbulent viscosity for low Reynolds flows.

A variation of the k-ω model is the SST k-ω model (Menter, 1994) which capitalizes on the accuracy of the k-ω model within the near-wall region and the k-ε model in the far-field region. Such an approach is done by transforming the k-ε model into a k-ω formulation and incorporating a blending function between the two regions. In addition, the transport of turbulent shear stress is accounted for by modifying the turbulent viscosity. As such, the SST k-ω model is able to model a wider range of flow profiles with increased accuracy.

SIMULATION MODEL

As mentioned above, the focus of this work was directed towards the offshore wind turbine industries. Hence, the simulation model was set up with reference to the Scroby Sand Wind Farm in the UK. The diameter of the cylinder was D = 4.2 m and the input velocity was 1.25 m/s which results in a Reynolds number of Re = 5.2 × 10^6. All simulations in this work were done on a 2D plane.

Model Geometrical Dimension and Mesh

The geometry of the computational domain used for the simulation was 25D × 20D. From the center of the cylinder, the velocity inlet boundary was 10D upstream while the outflow boundary was 15D downstream from the center of the cylinder. The upper and lower far-field symmetrical boundaries were 10D from the center of the cylinder. Figure 1 shows the geometrical dimensions of the computation domain.

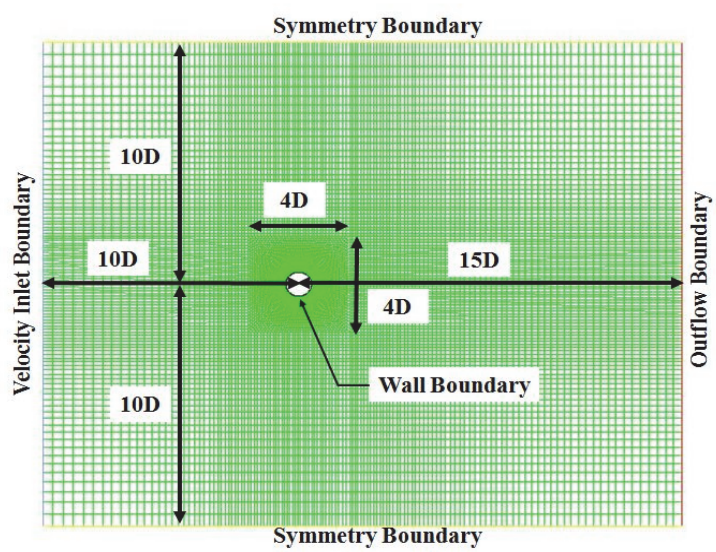

Figure 1: The geometrical dimensions and boundary conditions of the computational domain used in the simulations.

A hexahedral block mesh was used for all the simulations. The meshing of the model was divided into 2 zones, the inner zone which is a 4D × 4D block around the cylinder and the outer zone which is the zone away from the cylinder. For the inner zone, the grid expansion ratio ranged from 1.01 – 1.05 from the cylinder wall. As for the outer zone, the grid expansion ratio from the inner zone edge was constant at 1.02 downstream and 1.05 for the upper and lower far fields and upstream direction.

Boundary Conditions and Input Parameters

Zone	Boundary Condition	Input Parameter
Upstream	Velocity Inlet	u_x=1.25 m/s, u_y=0 m/s
Downstream	Outflow	u_x=free, u_y=free
Upper and Lower Far-Field	Symmetry	u_x=free, u_y=0 m/s
Cylinder	Wall	u_x=0 m/s, u_y=0 m/s

Table 1: Boundary Conditions and input variables for the simulations performed in this works.

The type of boundary conditions and parameters are shown in Table 1. For the inlet free stream flow, the input parameters were obtained from that of Jones *et al.* (1969) experiments. Hence, the turbulence intensity, $I = 0.17\%$, and the turbulence viscosity ratio, $\mu_t/\mu=1$, was used in the simulations performed. Subsequently, the turbulent kinetic energy (k), turbulent dissipate rate (ε) and specific dissipation rate (ω) was determined using Equation 14, 15 and 16.

$$k = \frac{3}{2}\left(u_{avg} I\right)^2 \tag{14}$$

$$\varepsilon = \rho C_\mu \frac{k^2}{\mu}\left(\frac{\mu_t}{\mu}\right)^{-1} \tag{15}$$

$$\omega = \rho \frac{k}{\mu}\left(\frac{\mu_t}{\mu}\right)^{-1} \tag{16}$$

where u_{avg} is the mean velocity and C_μ is an empirical constant.

Numerical Solution Procedure

FLUENT utilizes a Finite Volume Method approach to solve the governing equations. For this work done, a SIMPLE algorithm (Patankar and Spalding, 1972) was used for the velocity-pressure coupling and a second order upwind scheme (Barth and Jespersen, 1989) was used for the spatial discretization of the simulation done.

Mesh Sensitivity

A mesh sensitive study was done on each of the turbulence models evaluated to ensure grid independence for all the simulation results obtained. The percentage difference between the coefficient of drag (C_D), coefficient of lift root-mean-square value (C_{Lrms}) and Strouhal number (St) for the different grid sizes were less than 2% before a grid independence result was achieved. Table 2 shows the results of the grid sensitivity study.

Mesh Size (Elements)	C_D	Diff. (%)	C_{Lrms}	Diff.(%)	St	Diff. (%)
Spalart Allmaras (Vorticity)						
43380	0.344	0.44%	-	-	-	-
44436	0.346		-		-	
Spalart Allmaras (Strain/Vorticity)						
43380	0.830	0.10%	0.906	0.79%	0.305	0.00%
44436	0.831		0.914		0.305	
k-ε (Standard)						
227232	0.270	0.00%	0.0744	0.43%	0.446	0.32%
252522	0.270		0.0741		0.445	
k-ε (RNG)						
227232	0.307	0.33%	0.171	1.79%	0.368	0.62%
252522	0.306		0.168		0.370	
k-ε (Realizable)						
227232	0.313	0.16%	0.0788	0.34%	0.426	0.00%
252522	0.312		0.0790		0.426	
k-ω (Standard)						
227232	0.463	0.98%	0.408	1.71%	0.319	0.69%
252522	0.459		0.401		0.322	
k-ω (SST)						
227232	0.457	0.55%	0.185	0.78%	0.321	0.93%
252522	0.455		0.183		0.324	

Table 2: Results of the mesh sensitivity study of the simulations done

RESULTS AND DISSCUSSION

For this work, the key parameters used to evaluate each turbulence model are the coefficient of pressure (C_p), coefficient of drag (C_D), coefficient of lift root-mean-square (C_{Lrms}), angle of separation (θ) and the Strouhal number (St). These parameters are of significant interest to the industry as they provide not only the key elements to predict the loading on a structure due to the fluid flow (C_p, C_D, C_{Lrms}), but also provide a good quantitative description of the flow pattern (θ, St) around the structure.

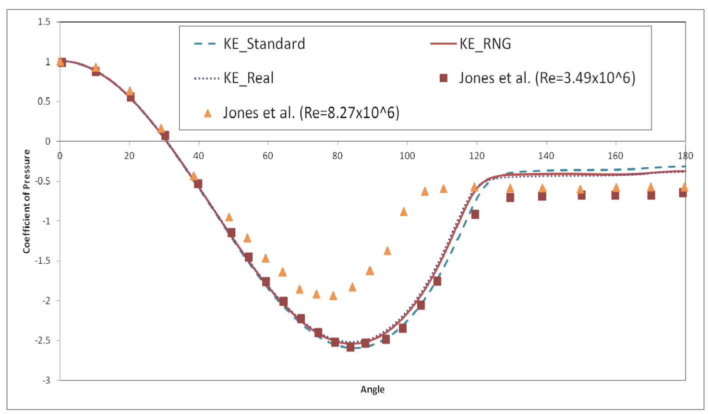

Figure 2: The coefficient of pressure (C_p) of the *k-ε* model simulation results plotted against experimental data obtained by Jones *et al.* (1969)

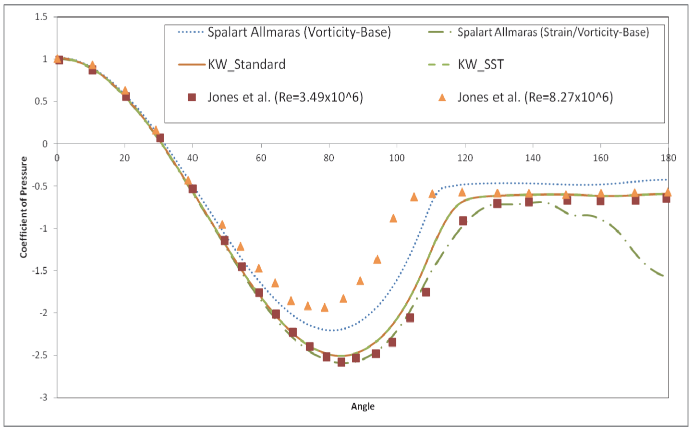

Figure 3: The coefficient of pressure (C_p) of the k-ω and Sparlart Allmaras model simulation results plotted against experimental data obtained by Jones *et al.* (1969)

The coefficient of pressure (C_p) of the simulation results is plotted against data obtained by Jones *et al.* (1969) in Figure 2 and 3. Although the C_p value of Jones *et al.* (1969) experiments for Re = 5.2×10^6 could not be obtained, that of Re = 3.49×10^6 and Re = 8.27×10^6 was available and provided a good benchmark to the simulation results. For the k-ε model and the k-ω model, the pressure distribution of the simulation results tends to overestimate the pressure around the upper and lower zones (at angle approx. 60° – 120°) of the cylinder, being closer to the pressure profile of the Re = 8.27×10^6 flow. For the leeward back-pressure (at angle 180°), k-ε model underestimates the pressure whereby both the Re = 3.49×10^6 and Re = 8.27×10^6 experimental flow converges to a C_p value of approximately -0.60. However, for the k-ω model, the back-pressure from the simulation results correlated very well with experimental data as seen in Figure 3.

The Spalart Allmaras model did not however capture the flow around the cylinder well. For the Spalart-Allmaras (Vorticity) model, although the pressure profile agreed reasonably well with experimental results, it must be noted that for this simulation, no vortex shedding was obtained. As for the Spalart-Allmaras (Strain/Vorticity) model, the flow around the upstream portion of the cylinder agreed reasonably with experimental values. However, upon flow separation (at angle approx. 120°) the model was no longer able to capture the flow accurately as seen by the fluctuating pressure profile at that leeward side of the cylinder.

In addition to the C_p, other flow parameters (θ, St, C_D , C_{Lrms}) were similarly analyzed in this work. Although seemingly independent, these flow parameters do share a close-coupled relationship with one another. For flows around a cylindrical bluff body, a key factor which influences the vortex shedding is the angle at which the flow separates around the cylinder. The larger the angle of separation, the narrower is the width of the vortex shedding and vice versa. A narrow wake region results in a shorter vortex period, which influences the Strouhal number, and results in a weaker negative back-pressure. The result of a reduction in the negative back-pressure similarly causes a decrease in the resultant coefficient of drag. A detailed description of the mechanism of a flow around the cylinder was presented by Sumer *et al.* (2006).

The angle of separation and coefficient of drag for the simulations as well as that observed in experimental work done by Achenbach *et al.* (1968), James *et al.* (1980), Schmidt *et al.* (1966) and Roshko *et al.* (1960) are shown in Table 3.

Model	Angle of Sep. (θ)	Coeff. Of Drag (C_D)
Spalart Allmaras (Vorticity)	113.18	0.354
Spalart Allmaras (Strain/ Vorticity)	120.00	0.830
k-ε (Standard)	123.47	0.270
k-ε (RNG)	121.83	0.307
k-ε (Realizable)	122.38	0.313
k-ω (Standard)	114.70	0.463
k-ω (SST)	109.76	0.457
Achenbach *et al.* (1968) Re=4.7×10^6	111.94	0.726
James *et al.* (1980) Re=5.46×10^6	110.94	0.317
Schmidt *et al.* (1966) Re=5.0×10^6	-	0.533
Roshko *et al.* (1960) Re=5.32×10^6	-	0.697

Table 3: The angle of separation and coefficient of drag obtained from the simulations performed and experimental data found in literature.

For the angle of separation, the k-ω models, in particular the k-ω (SST) models, agreed best with experimental data obtained from various groups. For the k-ε models, the simulation results showed that it tends to overestimate the angle of separation. Although only the standard wall function was used for all k-ε simulations, the authors did explore other wall functions, which are the Enhance Wall Function and the Non-Equilibrium Wall Function available in FLUENT (ANSYS FLUENT, 2011). However, similar separation angles of approximately 120° were obtained from these simulations using the alternative wall functions. For the Spalart Allmaras model, as mentioned earlier, the ability to capture the flow around a cylinder was not ideal. The data presented for both Spalart Allmaras models in Tables 3 and 4 are to provide a completeness to this study. However, it was interesting to note that for the Spalart-Allmaras (Vorticity) model, the angle of separation agreed reasonably well with experimental data despite not being able to capture the vortex shedding.

For the coefficient of drag, the inverse-relationship between the angle of separation and the C_D value can be seen in Table 3. As the angle of separation for each model increases, the corresponding C_D decreases. Based on the simulation results, both k-ω models agreed well with experimental data, falling within the range of experimental C_D values obtained by different groups. For the k-ε models, however, the C_D of the simulations is underestimated as compared to experimental data. This is primarily due to the large angle of separation obtained by this model.

The Strouhal number (St) and the coefficient of lift root-mean-square (C_{Lrms}) for the simulation results as well as experimental observations are Jones *et al.* (1969), Gunter (1983), Roshko *et al.* (1960) and Schmidt *et al.* (1966) presented in Table 4.

Model	Strouhal number (St)	Coeff. Of Lift rms (C_{Lrms})
Spalart Allmaras (Vorticity)	-	-
Spalart Allmaras (Strain/ Vorticity)	0.305	0.9063
k-ε (Standard)	0.446	0.0744
k-ε (RNG)	0.365	0.1702
k-ε (Realizable)	0.426	0.0788

k-ω (Standard)	0.320	0.4079
k-ω (SST)	0.321	0.1847
Jones *et al.* (1969) Re=5.61×10^6	0.253	0.1140
Gunter (1983) Re=5.25×10^6	0.262	0.0467
Roshko *et al.* (1960) Re=5.32×10^6	0.263	-
Schmidt *et al.* (1966) Re=5.0×10^6	-	0.1379

Table 4: The Strouhal number and coefficient of lift root-mean-square values obtained from the simulations performed and experimental data found in literature.

It is clear that all models overestimate the Strouhal number. However, of all the models, the k-ω model provides the closest agreement with experimental data primarily due to its good prediction of the angle of separation of the flow. The k-ε model significantly overestimates the Strouhal number due to the overestimation of the angle of separation which results in a narrower wake region and higher vortex frequency. For the coefficient of lift rms value, the k-ε model agrees well with the experimental data. While the k-ω models do overestimate the C_{Lrms}, there is still a reasonable agreement between the C_{Lrms} obtained with the k-ω (SST) models and that obtained experimentally by Schmidt *et al.* (1966).

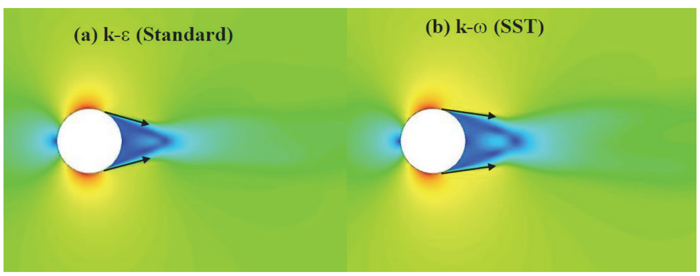

Figure 4: The mean velocity profile obtained from the k-ε (standard) and the k-ω (SST) models simulations.

To provide a clearer physical understanding of the simulation results using a pictorial approach, the mean velocity profile of k-ε (standard) and k-ω (SST) simulations are shown in Figure 4. Using the arrows in the figure as a gauge line, the late separation of the k-ε (standard) model results in a narrower wake width as compared to the k-ω (SST) model which has a slightly broader wake region. Hence, this difference in the wake region influences the flow properties and the model accuracy.

Based on the discussion presented, the major factor which determines the turbulence models accuracy in predicting the flow around a cylindrical bluff body is the angle of flow separation. From the simulation results, the k-ω model is able to capture the flow separation well, particularly the k-ω (SST) model where the angle of separation best correlates with experiments results. In addition, the k-ω (SST) model C_D values agree well with experimental data and the Strouhal number and C_{Lrms} having the closest agreement with experiments results as compared to the other models. With this good agreement with experimental data, when choosing a one- or two-equation RANS approach, the authors recommend the k-ω (SST) model for the flow around an extremely large cylinder.

For the k-ε models, the tendency to overestimate the flow separation angle results in the flow parameters for such a model to have a poorer agreement with experiment data as compared to the k-ω (SST) model. However, in consensus with Ong *et al.* (2009), the k-ε model does reasonably agree with experimental data and it can be applied for engineering purposes if need be. As for the Spalart-Allmaras model, while it requires a significantly short computational time due to the number of equations it has to solve and its coarse mesh, the ability to capture the flow separation around the cylinder is poor. It was noted that when the Spalart-Allmaras model only considered the vorticity magnitude in the turbulence production term, the resultant C_p and C_D predicted provided a reasonable agreement with the experimental data despite no vortex shedding being formed. Hence, a more detailed study will be done using this model to find an approach to reduce the simulation time for flows around large cylindrical bluff bodies.

CONCLUSIONS

In this work, the one- and two-equation RANS turbulence model was evaluated to determine the best approach to model the flow around an extremely large cylindrical bluff body. It was determined that the key parameter to be modeled to ensure accurate results is the angle of separation around the cylindrical bluff bodies. Based on the simulation results, the k-ω (SST) model agreed best with experimental data as compared to the other one- and two-equation turbulence models. Although the k-ε model agreed reasonability well with experimental data, the overestimation of the flow separation angle resulted in a poorer correlation with experimental observation as compared to the k-ω models. The Spalart-Allmaras model performed the poorest among all the turbulence models evaluated as it was not able to model the flow separation and vortex shedding well. However, the significantly short computational time and a reasonable agreement of C_p and C_D values when only vorticity was considered in the turbulence production term have given the authors motivation to explore this approach further.

ACKNOWLEDGEMENTS

The authors would like to acknowledge the support of the Energy Research Institute @ NTU (ERI@N) under the Offshore Renewables Joint Industry Programme (JIP) for their support in undertaking this work.

REFERENCES

Achenbach, E. (1968). "Distribution of local pressure and skin friction around a circular cylinder in cross-flow up to Re = 5×10^6," *J Fluid Mech*, Vol 34, pp 625-639.

ANSYS FLUENT (2011). *Theory Guide*, ANSYS Inc. 798 pp.

Barth, T.J and Jespersen, D. (1989). "The design and application of upwind schemes on unstructured meshes," *American Institute of Aeronautics and Astronautics*, Technical Report AIAA 89-0366.

Catalano, P, Wang, M, Gianluca, I,and Parviz, M. (2003). "Numerical simulation of the flow around a circular cylinder at high Reynolds numbers," *Int J Heat Fluid Fl,* Vol 24, pp 463-469.

Dacles-Mariani, J, Zilliac, G.G, Chow, J.S, and Bradshaw, P. (1995). "Numerical/Experimental study of a wingtip vortex in the near field," *AIAA J*, Vol 33, No 9, pp 1561-1568.

DECC (2008). *Dynamics of scour pits and scour protection- Synthesis report and recommendations (Milestones 2 & 3),*Final report prepared by HR Wallingford Ltd, ABPmer Ltd and CEFAS for the Research Advisory Group, Department of Energy and Climate Change (DECC) and Department for Environment, Food and Rural Affairs (Defra), 18pp.

Gunter, S. (1983). “On the force fluctuations acting on a circular cylinder in crossflow from subcritical up to transcritical Reynolds numbers,” *J Fluid Mech*, Vol 133, pp. 265-285.

James, W.D, Paris, S.W, and Malcolm G.N. (1980). “Study of viscous crossflow effects on circular cylinders at high Reynolds numbers,” *AIAA J*, Vol 18, No 9, pp 1066-1072.

Jones, G.W, Cincotta, J.J, and Walker, R.W. (1969). “Aerodynamics forces on a stationary and oscillating circular cylinder at high Reynolds numbers,” *NASA Technical Report*, NASA TR R-300, 62 pp.

Launder, B.E and Spalding, D.B. (1972). “Lectures in mathematical models of turbulence,” *Academic Press*, London, England, 169 pp.

Launder, B.E and Spalding, D.B. (1974). “The numerical computation of turbulent flows,” *Comput Meth Appl Mech Eng*, Vol 3, pp 269-289.

Menter, F.R. (1994). “Two-equation eddy-viscosity turbulence models for engineering application,” *AIAA J*, Vol 32, No 8, pp 1598-1605.

Ong, M.C, Utnes, T, Holmedal, L.E, Myrhaug, D, and Pettersen B. (2009). “Numerical simulation of flow around a smooth circular cylinder at very high Reynolds numbers,” *Mar Struct,* Vol 22, pp 142-153.

Patankar S.V and Spalding D.B. (1972). “A calculation procedure for heat, mass and momentum transfer in three-dimensional parabolic flows,” *Int J of Heat and Mass Transfer*, Vol 15, No 10, pp 1787-1806.

Roshko, A. (1960). “Experiments on the flow past a circular at very high Reynolds number,” *J Fluid Mech*, Vol 10, No 3, pp 345-356.

Schmidt, L.V. (1966). “Fluctuating force measurements upon a circular cylinder at Reynolds number up to 5×10^6,” *NASA Technical Report,* Document ID 19660022955, 17 pp.

Shih, T.H, Liou, W.W, Shabbir, A, Yang, Z and Zhu, J. (1995). “A new k-ε eddy-viscosity model for high Reynolds number turbulent flows – Model development and validation,” *Computers Fluids*, Vol 24, No 3, pp 227-238.

Spalart, P.R and Allmaras S.R. (1992). “A one equation turbulence model for aerodynamic flows,” *American Institute of Aeronautics and Astronautics*, Technical Report AIAA 92-0439.

Squires, K.D, Krishnan, V, and Forsythe, J.R. (2008). “Prediction of the flow over a circular cylinder at high Reynolds number using detached-eddy simulation,” *J Wind Eng Ind Aerod*, Vol 96, pp 1528-1536.

Sumer B.M and Fredsøe, J. (2006). *Hydrodynamics around cylindrical structures*, World Scientific Publishing, 530 pp.

Unal, U.O and Goren O. (2006). “Vortex shedding from a circular cylinder at high Reynolds number,” *Proc 11th Int Congress of the Int Maritime Assn. of the Mediterranean*, Lisbon, Maritime Transportation and Exploitation of Ocean and Coastal Resources, Vol 2, pp 301–307.

Wilcox, D.C. (1988). "Re-assessment of the scale-determining equation for advanced turbulence models," *AIAA J*, Vol 26, No 11, pp 1299-1310.

Yakhot, V and Orszag, S.A. (1986). “Renormalization group analysis of turbulence: I. Basic Theory,” *J Sci Comput*, Vol 1,No 1, pp 1-51.